Chinese Chemical Letters 34 (2023) 107298

Contents lists available at ScienceDirect

Chinese Chemical Letters

journal homepage: www.elsevier.com/locate/cclet

One-step fabrication of mesoporous sulfur-doped carbon nitride for highly selective photocatalytic transformation of native lignin to monophenolic compounds

Conghao Ku[a,b,c], Huiqin Guo[a,c,*], Kexin Li[a,b,c,*], Qiong Wu[a], Liushui Yan[a,c,*]

[a] Key Laboratory of Jiangxi Province for Persistent Pollutants Control and Resources Recycle, Nanchang Hangkong University, Nanchang 330063, China
[b] National-Local Joint Engineering Research Center of Heavy Metals Pollutants Control and Resource utilization, Nanchang Hangkong University, Nanchang 330063, China
[c] Jiangxi Provincial Experimental Teaching Demonstration Center of Environmental Science and Engineering, Nanchang Hangkong University, Nanchang 330063, China

ARTICLE INFO

Article history:
Received 19 November 2021
Revised 17 January 2022
Accepted 4 March 2022
Available online 7 March 2022

Keywords:
Mesostructure
Sulfur-doped carbon nitride
Photocatalysis
Lignin model compound
Native lignin
Monophenolic compounds

ABSTRACT

Photocatalytic selective transform native lignin into valuable chemicals is an attractive but challenging task. Herein, we report a mesoporous sulfur-doped carbon nitride (MSCN-0.5) which is prepared by a facile one-step thermal condensation strategy. It is highly active and selective for the cleavage $C_\alpha-C_\beta$ bond in $\beta-O-4$ lignin model compound under visible light radiation at room temperature, achieving 99% substrate conversion and 98% $C_\alpha-C_\beta$ bond cleavage selectivity. Mechanistic studies revealed that the $C_\beta-H$ bond of lignin model compounds activated by holes and generate key C_β radical intermediates, further induced the $C_\alpha-C_\beta$ bond cleavage by superoxide anion radicals ($^{\bullet}O_2^-$) to produce aromatic oxygenates. Waste *Camellia oleifera* shell (WCOS) was taken as a representative to further understand the reaction mechanisms on native lignin. 33.2 mg of monophenolic compounds (Vanillin accounted for 22% and Syringaldehyde for 34%) can be obtained by each gram of WCOS lignin, which is 2.5 times as that of the pristine carbon nitride. The present work offers useful guidance for designing metal-free heterogeneous photocatalysts for $C_\alpha-C_\beta$ bond cleavage to harvest monophenolic compounds.

The depletion of fossil fuels has animated scientists to develop new technologies for producting fuels and chemicals from lignocellulosic biomass [1,2]. Lignin is the most abundant aromatic biopolymer in lignocellulosic biomass that can be transformed to phenolic monomers [3]. However, its complex irregular polymeric structure renders it challenging to be transformed. The main obstacle of lignin transformation is the selective cleavage of the C–O or C–C bonds in lignin linkages [4–6]. Some strategies have succeeded in breaking almost all target C–O bonds, mainly $\beta-O-4$ bonds, to produce the aromatic products [7–10]. C–C bonds are generally left untouched due to its high bond dissociation energy, which limits theoretical aromatic monomer yield. In addition, C–C bonds can be survived in most conventional lignin depolymerization conditions, even in a high temperture (more than 250 °C) [11]. Thus, breaking C–C bonds in lignin (especially $C_\alpha-C_\beta$ bonds) is one of the key challenges for the valorization of lignin. Only few thermocatalytic methods, majorly aerobic oxidation based on metal complexes was reported that can cleaving the stable $C_\alpha-C_\beta$ bonds [12]. Besides, additional additives such as expensive oxidants are typically required during the reaction. Therefore, it is challenging but attractive that developing a green technique for selective cleaving $C_\alpha-C_\beta$ bonds in lignin under mild condition to harvest valuable chemicals such as vanillin and syringaldehyde.

Photocatalysis has been emerged as a promising technique for green oxidation, which can produce oxidation species such as photogenerated holes and superoxide anion radicals under light irradiation without auxiliary of additional oxidants. Due to the intimate contact with lignin macromolecules, several homogeneous photocatalysts have been reported for $C_\alpha-C_\beta$ bonds cleavage with high conversion and selectivity, such as ruthenium (Ru)-, copper (Cu)- and vanadium (V)-based photocatalysts [13–15]. But the use of homogenous photocatalysts makes it difficult to the separation of aromatic products and recycle of catalysts. Thus, increasing research have been shifted to heterogeneous photocatalysts. How-

* Corresponding authors at: Key Laboratory of Jiangxi Province for Persistent Pollutants Control and Resources Recycle, Nanchang Hangkong University, Nanchang 330063, China.
E-mail addresses: guohuiqin@nchu.edu.cn (H. Guo), likx@nchu.edu.cn (K. Li), yanliushui@nchu.edu.cn (L. Yan).

https://doi.org/10.1016/j.cclet.2022.03.021
1001-8417/

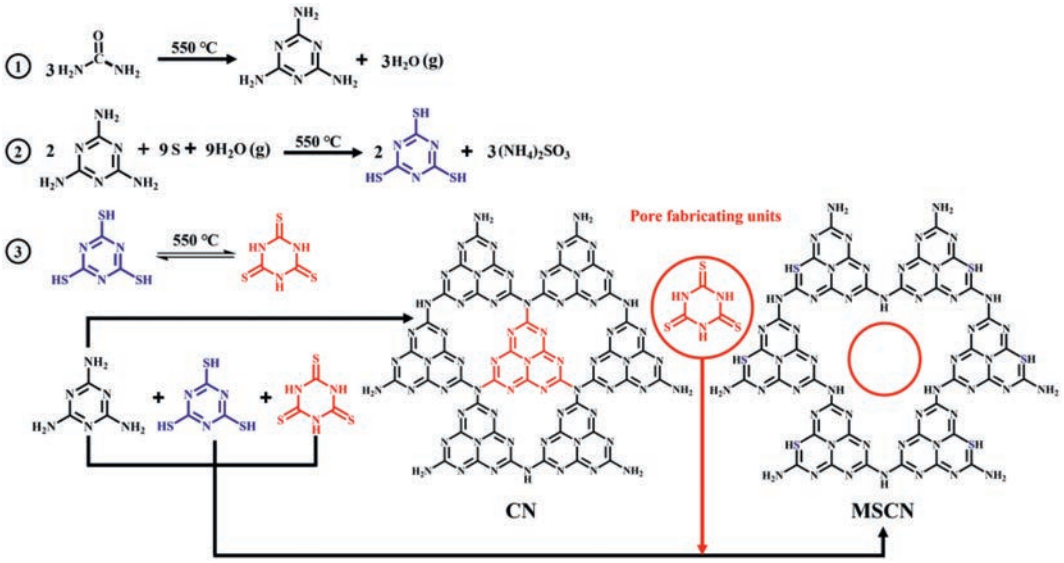

Scheme 1. Fabrication mechanism of mesoporous sulfur-doped carbon nitride.

ever, the lack of intimate contact between heterogeneous photocatalysts and lignin macromolecules, and the inappropriate energy band structure of the photocatalyst, creating a barrier for the cleavage of $C_\alpha-C_\beta$ bonds. Although few heterogeneous photocatalysts have been fabricated for the effective breaking of $C_\alpha-C_\beta$ bonds [16], it is extremely meaningful to develop high active heterogeneous photocatalyst for highly selective cleavage of $C_\alpha-C_\beta$ bonds.

Graphitic carbon nitride (g-C_3N_4) is a promising metal-free heterogeneous photocatalyst for photocatalytic selective cleavage of $C_\alpha-C_\beta$ bonds, based on the $\pi-\pi$ stacking interactions between the triazine rings of g-C_3N_4 and benzene rings of lignin model compounds [17]. However, due to the serious photogenerated carriers recombination, insufficient active sites and the inappropriate energy band structure, the photocatalytic activity and selectivity for the $C_\alpha-C_\beta$ bonds cleavage by the pristine g-C_3N_4 was very low. In particular, the number of active sites and the energy band structure also affect the photocatlytic activity and selectivity.

Constructing porous microstructure is an effective strategy to increase the number of the active sites in g-C_3N_4 [18]. And nonmetallic doping has been widely used to adjust the energy band structure of g-C_3N_4 [19–21]. Traditional synthetic method of mesoporous sulfur-doped carbon nitride (MSCN) usually require hydrothermal pretreatment [22], or use SiO_2 nanoparticles as hard templates and following removal of them by etching with HF solution [23]. Different from these methods, the sublimed sulfur is innovatively used as both pore-forming agent and sulfur doping substance in this work, and MSCN is initially planned to be prepared *via* one-step thermal condensation strategy. Interestingly, it found that the energy band structures of the MSCN can be tuned by controlling the mass ratio (*X*) of sublimed sulfur to urea in the precursor, matching the redox potential required by the cleavage of $C_\alpha-C_\beta$ bonds. The $\beta-O-4$ lignin model compound was employed to study the structure-performance relation of MSCN-*X*.

Up to now, most studies used lignin model compounds as substrate to study the photocatalytic cleavage mechanisms of lignin bonds. The transformation of native lignin to value-added chemicals and the understanding on the reaction mechanisms about is very limited. Waste *Camellia oleifera* shell (WCOS) is a main byproduct of the *Camellia* seed oil processing industry. As a typical waste biomass, it composed of high content of lignin but is usually discarded or burned directly. In our previous works, it was mainly used as raw material to study the high value utilization of waste biomass [24]. In this work, the lignin extracted from the WCOS was employed as the native lignin to promote the understanding of the photocatalytic reaction mechanisms.

The MSCN-*X* were prepared *via* one-step thermal condensation (Supporting information Part I). Fabrication mechanism of MSCN-*X* is shown in Scheme 1. In the case of high temperatures, part of melamine produced from urea will undergo a disproportionation reaction with sublimed sulfur and water vapor, producing trithiocyanuric acid and $(NH_4)_2SO_3$. Typically, trithiocyanuric acid existed in two isomeric forms, *i.e.*, *s*-triazine-2,4,6-trithiol and 1,3,5-triazinane-2,4,6-trithione. The trithione form cannot react with $-NH_2$ groups so that abundant mesopores was produced in the framework of CN. The trithiol form can react with melamine to produce sulfur-dopped tri-*s*-triazine units and produced MSCN-*X* by condensation of $-NH_2$ groups.

The chemical structure of the prepared CN and MSCN-0.5 was first characterized by X-ray diffraction (XRD) patterns (Fig. 1a). the XRD patterns of MSCN-0.5 were very similar to that of CN, indicating the general structure of carbon nitride was preserved after the sulfur doping. Two distinguish peaks centered at 13.1° and 27.5° were matched with the in-plane repeated heptazine units and the stacking inter layer, respectively [25]. Compared with CN, the left shift of (002) peak of MSCN-0.5 suggested that the increase of interlamellar spacing.

The morphologies and microstructures of the prepared materials were observed under the transmission electron microscopy (TEM) images. As shown in Fig. 1b, CN appeared a smooth 2D sheet-like structure, which was attributed to that the framework of CN is formed by continuous polycondensation of $-NH_2$ groups between the tri-*s*-triazine units. Different from CN, the MSCN-0.5 appeared a layered microstructure with abundant pores (Fig. 1c), which may attribute to the existence of pore-fabricating units that hindered the continuous polycondensation of tri-*s*-triazine units [26]. The N_2 adsorption-desorption isotherm data also confirmed this result (Figs. S1 and S2 in Supporting information). All samples have a typical type IV isotherm with a H3-type hysteresis loop, indicating the mesopores existed in these two solid materials. The mesopores in CN were attributed to the interspace formed by the stacking of carbon nitride sheets. And those in MSCN-0.5 were mainly attributed to the mesopores on carbon nitride sheets surface. Compared to the CN (52.3 m^2/g), MSCN-0.5 shows a higher of specific surface area (105.7 m^2/g), which will provide more active sites in the reaction.

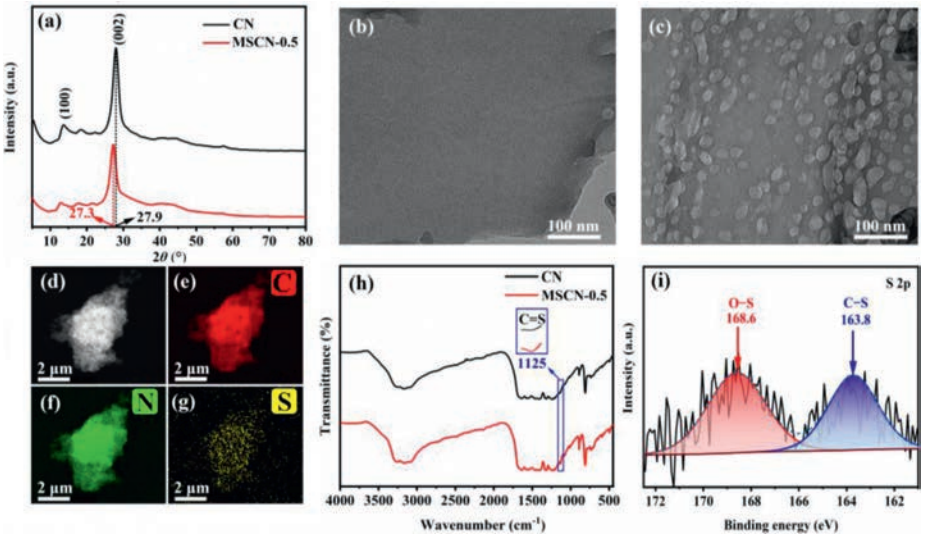

Fig. 1. (a) XRD pattern of prepared photocatalysts. (b) TEM image of CN. (c) TEM image of MSCN-0.5. (d–g) EDX elemental mapping of MSCN-0.5. (h) FT-IR spectra of MSCN-0.5. (i) XPS high-resolution spectra of S 2p of MSCN-0.5.

The introduction of sulfur in the catalysts was revealed by EDX element mapping (Figs. 1d-g), Fourier transform infrared (FT-IR) (Fig. 1h) and X-ray photoemission spectroscopy (XPS) analysis (Fig. 1i). The EDX element mapping of MSCN-0.5 shows a uniform distribution of C, N and S throughout the whole selected area, reflecting the uniform doping of sulfur in MSCN-0.5. According to the results of FT-IR, the peaks located in 1200–1600 cm^{-1} belong to the stretching vibration of the aromatic C–N in heterocyclic triazine ring, and the typical peak centered at 807 cm^{-1} is ascribed to the bending vibration of tri-*s*-triazine subunits [27]. The absorption band in the range of 3000–3500 cm^{-1} can be originated from the $-NH_2$ or $-NH$ functional groups at the edge of carbon nitride and the adsorbed H_2O molecules [28]. Notably, compared with CN, MSCN-0.5 displayed an additional peak at 1125 cm^{-1}, which attributed to the stretching vibration of C=S bonds, revealing that the N elements in the tri-*s*-triazine subunits were replaced by S elements [29]. The high-resolution XPS S 2p spectra showed that two peaks located at 168.6 and 163.8 eV, which corresponding to the S–O bond and C–S bond, respectively [30–32]. The peak at 163.8 eV is originated from the formed C–S bonds in MSCN-0.5. And that centered at 168.6 eV is ascribed to the S–O bonds of ammonium sulfite or sulfate, which was produced from the calcination treatment under air atmosphere [33,34]. The content of S atoms on the surface of the MSCN-0.5 from XPS is 0.17 wt% (Table S1 in Supporting information). All above results revealed that the N atoms in the tri-*s*-triazine subunits were replaced by S atoms. Besides, solid-state ^{13}C NMR spectra of the CN and MSCN-0.5 were studied to verify the internal structures (Fig. S3 in Supporting information). The peaks at 165.4 and 157.1 ppm of CN were assigned to the CN_3 (C_1) and $CN_2(NH_2)$ groups (C_2). Similar peaks were also observed in the MSCN-0.5, where the peak shifts were influenced by S doping [18,35].

In addition, to further investigate the substitution sites of S atoms in tri-*s*-triazine subunits, the high-resolution XPS spectra of the C 1s region and N 1s region for the CN and MSCN-0.5 were analyzed. As shown in Fig. S4 and Table S2 (Supporting information), for the CN, the XPS peak of C 1s centered at 284.8 and 288.2 eV were assigned to reference carbon element and sp^2-hybridized carbon bonded to nitrogen (N–C=N) [36]. For MSCN-0.5, the C 1s peak of N–C=N exhibited a slightly lower movement (0.10 eV) to 288.09 eV, indicating the improved electron density around C atom. This was due to the nitrogen atom (strong electronegativity) in N–C=N being replaced with sulfur atoms (weak electronegativity). To further confirm this point, the N 1s spectra of catalysts were studied. For CN, peaks at 398.67, 399.83, 401.18 and 404.52 eV were attributed to the sp^2 hybridized N atoms in heterocycle (C–N=C, marked as N_{2C}), tertiary N bonded to C atoms in the form of $(N-(C)_3$, marked as N_{3C}), amino functional groups ($-NH_x$) and π-excitations, respectively [37,38]. Compared with the N_{3C}/N_{2C} atomic ratio of CN and MSCN-0.5, it increased from 0.40 to 0.45 after the S doping, indicating the decrease in relative content of N_{2C} atom in the framework. These results were further confirmed that the N atom in C–N = C was substituted by S atom.

The optical absorption and band structure of the prepared samples were investigated by Ultraviolet-visible diffuse reflectance spectrum (UV–vis DRS). As shown in Figs. S5 and S6 (Supporting information), a red shift in the absorption edge was achieved in MSCN-*X*. Sulfur doping could not only enhance the visible light absorption, but also decrease the band-gap energy of the catalyst. With an increase in the value of *X* from 0.1 to 1.0 in MSCN-*X*, the band-gap energy gradually decreased from 2.70 eV to 2.55 eV. To further investigate the energy band structures of catalysts, the CB potentials (E_{CB}) were roughly determined by Mott-Schottky measurements (Fig. S7 in Supporting information). The flat-band potentials (E_{fb}) of MSCN-*X* were shifted from −0.84 V to −0.94 V (*vs.* Ag/AgCl) upon increasing the value of *X* from 0.1 to 1.0, which are equivalent to from −0.64 V to −0.74 V (*vs.* NHE) [39]. Considering that the conduction band minimum (CBM) of n-type semiconductor is 0.1 V negative than E_{fb} [40], the CBMs of MSCN-*X* were calculated to shift from −0.74 V to −0.84 V (*vs.* NHE), and the valence-band maximum (VBM) of MSCN-*X* was shifted from 1.96 V to 1.71 V (*vs.* NHE) upon increasing the value of *X* from 0 to 1.0. The energy band structure of the prepared photocatalysts was shown in Fig. S8 (Supporting information). The VBM is mainly determined by the s-orbitals and p-orbitals of N atom [41], these results proved that S 2p orbitals of S atoms in MSCN-*X* could take part in the formation of VBM and CBM.

In addition to adjusting the band structure, the introduction of sulfur in MSCN-*X* can also influence the separation and transfer of photoexcited charge carriers. Firstly, the charge separation of the prepared catalysts was investigated by the photoluminescence (PL) spectra that were measured with an excitation wavelength at 375 nm. As shown in Fig. S9 (Supporting information), the lowest PL peak intensity of MSCN-0.5 indicated the highest charge separation efficiency [42,43]. Moreover, the time-resolved transient PL decay spectra was shown in Fig. S10 (Supporting infor-

mation) and the corresponding emission lifetime (τ) were listed in Table S3 (Supporting information). Both the short-lifetime component ($\tau_1 = 1.53$ ns) and the long-lifetime component ($\tau_2 = 6.84$ ns) of MSCN-0.5 are much smaller than that of CN ($\tau_1 = 2.08$ ns, $\tau_2 = 8.02$ ns), indicating that sulfur doping decreased the recombination number of photo-generated electron-hole pairs in MSCN-0.5 [44]. As a representative of the overall decay behavior, the average PL lifetime of CN and MSCN-0.5 is 5.49 ns and 4.73 ns, respectively. Transient photocurrent measures (Fig. S11 in Supporting information) and electrochemical impedance spectrum (EIS) (Fig. S12 in Supporting information) were measured to further investigate the transmission of photo-generated charges. Compared with CN, MSCN-0.5 exhibited a satisfactory photocurrent response and a representative Nyquist plot with a much smaller arc radius, further confirming that sulfur doping can accelerate the surface migration of photogenerated carrier.

To study the photocatalytic $C_\alpha-C_\beta$ bond cleavage reaction and evaluate the photocatalytic activity and selectivity of MSCN-X, lignin model compound with $C_\alpha-OH$, $C_\alpha-C_\beta$, and $C_\beta-O$ bonds (2-phenoxy-1-phenylethanol) (**1a**), was typically used as a substrate in this work. The photocatalytic reactions in this work were all carried out in a customized quartz photocatalytic reactor under 425 nm LED blue light irritation, and the reactants were continuously stirred by magnetic forces during the whole photocatalytic reaction (Fig. S13 in Supporting information). Detailed quantitative methods and calculation formulas were shown in Supporting information Part I. Experiments and Results with different catalysts and reaction conditions are shown in Scheme S1 and Table S4 (Supporting information). As can be seen from these results, the photocatalytic reaction did not occur in the absence of photocatalyst or light illumination (Table S4, entries 1 and 10). The MSCN-0.5 confers remarkably higher photoactivity than CN, achieving a nearly completed conversion (99%) with a 98% of $C_\alpha-C_\beta$ bond cleavage selectivity (Table S4, entries 2–7). These results attribute to the higher specific surface area, higher charge separation efficiency, and smaller resistance of MSCN-0.5 than that of CN. The cleaved products include benzaldehyde (**1**), phenyl formate (**2**), phenol (**3**), and 2-phenoxy-1-phenylethanone (**4**). And the high $C_\alpha-C_\beta$ bond cleavage selectivity of MSCN-0.5 indicated that the energy band structure of MSCN-0.5 is more suitable for the redox potential required for $C_\alpha-C_\beta$ bonds cleavage. Moreover, reaction solvent experiments revealed that acetonitrile was the most suitable solvent for this photocatalytic reaction (Table S4, entries 8 and 9). And the recyclability experiments showed that a substrate conversion of 94% was obtained after four recycles of the MSCN-0.5 (Fig. S14 in Supporting information). After washing and drying treatment, the morphology and chemical state of MSCN-0.5 was characterized by TEM and XPS (Figs. S15 and S16 in Supporting information) analysis, it did not find obvious change of the porous microstructure and C−S bonds in the framework of MSCN, indicating a high stability of the structure of catalyst.

The radical quenching tests (Fig. S17 in Supporting information) and the electron spin resonance (ESR) (Figs. S18 and S19 in Supporting information) were carried out to investigate the photocatalytic reaction mechanism. Considering that the acetonitrile was employed as solvent for this photocatalytic reaction, and the VBM of MSCN-0.5 (1.83 V) is less positive than the oxidation potential (2.30 V) to produce hydroxyl radical ($^{\bullet}OH$) from H_2O, indicating that $^{\bullet}OH$ cannot be produced over MSCN-0.5. Moreover, Fig. S17 revealed that O_2 is indispensable for photocatalytic cleavage of $C_\alpha-C_\beta$ bonds. The CBM of MSCN-0.5 (−0.8 V) is more negative than the reduction potential (−0.33 V) for the conversion of O_2 to the superoxide radical ($^{\bullet}O_2^-$). This suggests that the photogenerated electrons from MSCN-0.5 can readily drive the generation of $^{\bullet}O_2^-$. In addition, *p*-benzoquinone (*p*-BQ), *tert*–butanol (*t*-BuOH) and triethylamine (TEA) were adopted as the scavengers for $^{\bullet}O_2^-$, $^{\bullet}OH$ radical and photo-generated holes (h^+), respectively. It found that the h^+ and $^{\bullet}O_2^-$ are essential active species for the reaction. *In-situ* ESR technique was used to further determine the active radicals produced in reaction process using DMPO and TEMPO as trapping agents. The quadruple peaks of DMPO-O_2^- emerged for MSCN-0.5 photocatalyst under visible light illumination, confirming the generation of $^{\bullet}O_2^-$ radicals (Fig. S18). And in Fig. S19, triple peak with intensity ratio of 1:1:1 for the TEMPO-h^+ adducts is observed in the MSCN-0.5, indicating h^+ participate in the photocatalytic reaction [45]. The results of ESR further confirmed that h^+ and $^{\bullet}O_2^-$ play a vital role in the photocatalytic reaction.

In addition, different from the results reported by Wang *et al.* [17], both benzaldehyde and phenyl formate can keep stable in our photocatalytic conditions (Eqs. 1 and 2 in Scheme S2 in Supporting information). This result can be attributed to that MSCN-0.5 has a more negative VB and CB potential than that of CN, which can prevent the further oxidation of photocatalytic products. Acetophenone was not detected and the formation of phenol in photocatalytic reaction indicated that the cleavage of $C_\alpha-C_\beta$ bonds in $\beta-O-4$ lignin model compounds accompanied with the partial cleavage of $C_\beta-O$ bonds (Fig. S20 in Supporting information).

Lastly, different lignin dimer model compounds were employed to determine the dehydrogenation sites of **1a**. Low conversion of 2-phenoxy-1-phenylethanone (**4**) indicated that it was not the intermediate of the photocatalytic reaction, and H-abstraction from $C_\alpha-H$ bond is not a major step (Eqs. 4 and 2 in Scheme S2 in Supporting information). The observation that the 2-phenoxy-1-phenylethane (**1b**) could not be converted suggested that the hydroxyl group connecting with α-C is necessary for the cleavage of the $C_\alpha-C_\beta$ bonds (Eq. 5 in Scheme S2 in Supporting information). Furthermore, the production of phenol acetate (**6**) from the depolymerization of 2-phenoxy-1-phenylpropan-1-ol (**1c**) confirmed that the dehydrogenation sites of lignin are in β-C (Eq. 6 in Scheme S2 in Supporting information).

Based on all the above analysis, we proposed a tentative reaction mechanism including of three different reaction routes which taking lignin model compound **1a** as an example (Fig. 2). The first reaction route is that the hydrogen of β-C was abstracted hole to generate a C_β-centered radical. The $^{\bullet}O_2^-$ radical and H^+ then adds to the C_β-centered radical (**3a**), forming an unstable six-membered ring intermediate (**4a**). The subsequent electron transfer in intermediate through a six-membered ring transition state would induce the elimination of H_2O and the cleavage of $C_\alpha-C_\beta$ and O−O bond, resultant of the benzaldehyde (**1**) and phenyl formate (**2**) formation [17,46]. The second reaction route is that the $C_\alpha-C_\beta$ bond and $C_\beta-O$ bond in part of the unstable six-membered ring intermediates (**4a**) break simultaneously and produce the benzaldehyde (**1**), formic acid (**5**) and phenol (**3**). And the formic acid and phenol produced were further degraded to CO_2 and H_2O. The third reaction route is that hydrogen abstraction from the $C_\alpha-H$ bond by the photo-generated holes gives a C_α-centered radical (**2a**) that can undergo a further hydrogen abstraction from the O−H bond to produce the ketone product (**4**) [47].

According to the above photocatalytic mechanism, the $C_\beta-H$ bond of lignin can be activated by the photogenerated holes and generate key C_β radical intermediates, further inducing the $C_\alpha-C_\beta$ bond cleavage to produce aromatic aldehydes in the participation of superoxide anion radicals ($^{\bullet}O_2^-$). Therefore, to further promote the understanding of the reaction mechanisms, real lignin extracted from the waste *Camellia oleifera* shell was employed as the substrate to conduct the catalytic reactions. The purity of WCOS lignin was 90.76% (expressed by Klason lignin) (Tables S5 and S6 in Supporting information), and the mole ratio of three basic structural units in WCOS lignin determined by the alkaline nitrobenzene oxidation method was G:S:H = 52.86:45.28:1.85 (Table S7 in Supporting information).

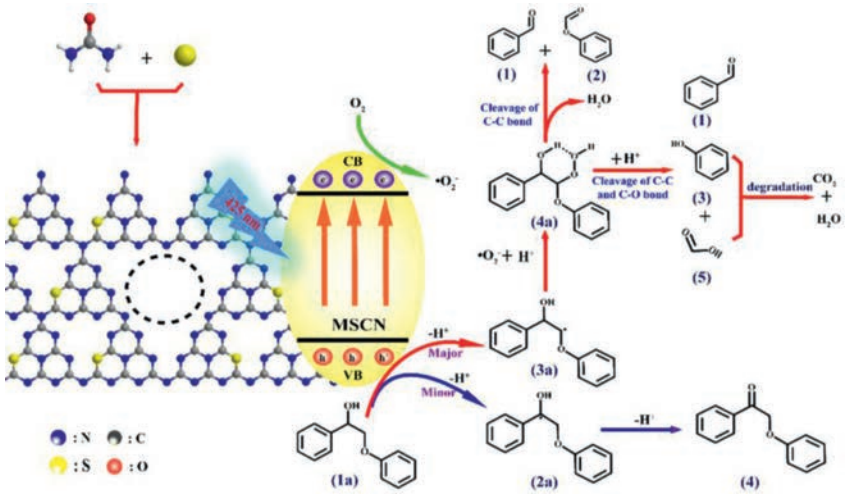

Fig. 2. Proposed photocatalytic reaction mechanism of the depolymerization of lignin model compound **1a**.

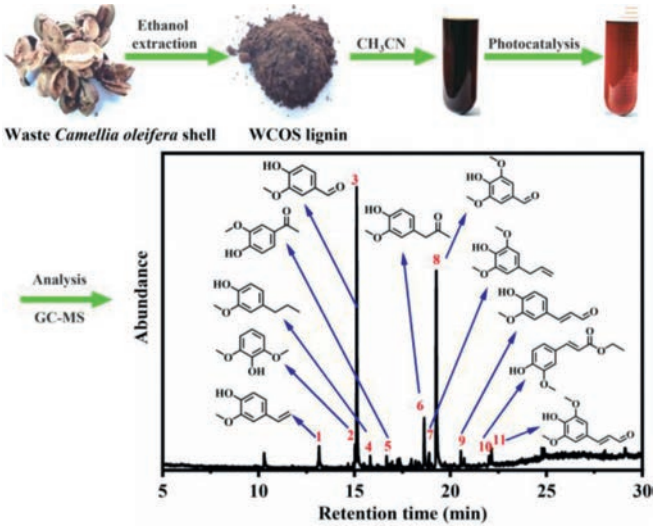

Fig. 3. Reaction process images and GC–MS total ion chromatograms of products obtained from the photocatalytic depolymerization of WCOS lignin. Reaction conditions: 150 mg of WCOS lignin, 75 mg of MSCN-0.5, 30 mL of CH3CN, air atmosphere, 20 W LED (centered at 425 nm), room temperature, irradiate 6 h.

The photocatalytic depolymerization process is illustrated in Fig. 3. The brown WCOS lignin solution in CH_3CN was decolored after the reaction, indicating the reduced molecular weight of the lignin molecule [48–50]. And according to the total ion chromatogram results of GC–MS for the products analysis, there are 11 monophenolic compounds identified (Part II in Supporting information). It is worth mentioning that parts of these monophenolic compounds, especially vanillin and syringaldehyde, belong to high-value chemicals, which provided direct evidence for lignin valorization to functionalized aromatics in our work. The production of aromatic aldehydes further verified the rationality of the proposed photocatalytic mechanism.

The products formation in the experimental conditions were quantified by GC–MS with an external standard method. As shown in Fig. S21 (Supporting information), it was found that MSCN-0.5 exhibited the best photocatalytic performance for depolymerization of lignin, with a total yield of monophenolic compounds of 26.3 mg/g lignin. To further improve the yield of monophenolic compounds, the reaction conditions were optimized. Under optimal conditions (5 g/L of WCOS lignin, 75 mg of MSCN-0.5, irradiation time = 7 h), each gram of WCOS lignin can achieve 33.2 mg of monophenolic compounds (Vanillin accounted for 22% and Syringaldehyde for 34%), which is 2.5 times higher than that of CN (13.2 mg/g lignin) (Fig. S22 in Supporting information). Furthermore, the G-units/S-units mole ratio of the products under this condition was calculated to be 1.24 (Table S8 in Supporting information), close to the composition of real lignin (G-units/S-units mole ratio in WCOS lignin was 1.17), suggesting that the mesoporous sulfur-doped carbon nitride could high selectively depolymerize WCOS lignin to monophenolic compounds.

In conclusion, a series of mesoporous sulfur-doped carbon nitrides with controllable energy band structures are successfully synthesized *via* one-step thermal condensation strategy and applied in the selective photocatalytic conversion of lignin to monophenolic chemicals. The energy band structure of MSCN-*X* can be tuned directly by controlling the mass ratio of sublimed sulfur to urea in the precursor (*X*). It found that MSCN-0.5 was powerful for photocatalytic cleavage of $C_\alpha-C_\beta$ bonds in lignin. Aromatic aldehydes with high yields of 98% were obtained from the conversion of $\beta-O-4$ lignin model compounds under visible light at room temperature. Mechanisms study for the $C_\alpha-C_\beta$ bond cleavage reaction suggested that the main process starts with photogenerated hole oxidation to produce C_β radical intermediate, which undergoes $C_\alpha-C_\beta$ bond cleavage by reacting with $^{\bullet}O_2^-$, further inducing the $C_\alpha-C_\beta$ bond cleavage to produce aromatic aldehydes. For photocatalytic depolymerization of native lignin, each gram of WCOS lignin can achieve 33.2 mg of monophenolic compounds (Vanillin accounted for 22% and Syringaldehyde for 34%). This study may shed light on designing low cost and nontoxic metal-free heterogeneous photocatalysts for effectively transforming native lignin to monophenolic compounds.

Declaration of competing interest

The authors declare no conflicts of interests.

Acknowledgments

This work was finacially supported by the National Natural Science Foundation of China (Nos. 21966023, 21665018 and 51568049), the Natural Science Foundation of Jiangxi Province, China (No. 20171ACB21035) and Jiangxi Province Graduate Student Innovation Special Fund (No. YC2020-S513).

Supplementary materials

Supplementary material associated with this article can be found, in the online version, at doi:10.1016/j.cclet.2022.03.021.

References

[1] X.J. Wu, X.T. Fan, S.J. Xie, et al., Nat. Catal. 1 (2018) 772–780.
[2] J. Gong, A. Imbault, R. Farnood, Appl. Catal. B: Environ. 204 (2017) 296–303.
[3] C.L. Chio, M. Sain, W.S. Qin, Renew. Sust. Energ. Rev. 107 (2019) 232–249.
[4] C. Xu, R.A. Arancon, J. Labidi, R. Luque, Chem. Soc. Rev. 43 (2014) 7485–7500.
[5] S. Gazi, Appl. Catal. B: Environ. 257 (2019) 117936.
[6] X. Shen, Y. Xin, H. Liu, B. Han, ChemSusChem 13 (2020) 4367–4381.
[7] J. Lu, M. Wang, X. Zhang, A. Heyden, F. Wang, ACS Catal. 6 (2016) 5589–5598.
[8] N. Luo, M. Wang, H. Li, et al., ACS Catal. 7 (2017) 4571–4580.
[9] G. Magallanes, M.D. Kärkäs, I. Bosque, et al., ACS Catal. 9 (2019) 2252–2260.
[10] H. Yoo, M.W. Lee, S. Lee, et al., ACS Catal. 10 (2020) 8465–8475.
[11] M.V. Galkin, J.S. Samec, ChemSusChem 9 (2016) 1544–1558.
[12] E. Subbotina, T. Rukkijakan, M.D. Marquez-Medina, et al., Nat. Chem. 13 (2021) 1118–1125.
[13] T. vom Stein, T. den Hartog, J. Buendia, et al., Angew. Chem. Int. Ed. 54 (2015) 5859–5863.
[14] X. Liu, H. Xu, Z. Ma, et al., RSC Adv. 6 (2016) 27126–27129.
[15] Y. Ma, Z. Du, J. Liu, F. Xia, J. Xu, Green Chem. 17 (2015) 4968–4973.
[16] X. Wu, J. Lin, H. Zhang, et al., Green Chem. 23 (2021) 10071–10078.
[17] H. Liu, H. Li, J. Lu, et al., ACS Catal. 8 (2018) 4761–4771.
[18] F. Li, X. Yue, H. Zhou, J. Fan, Q. Xiang, Chin. J. Catal. 42 (2021) 1608–1616.
[19] Y. Li, X. Li, H. Zhang, J. Fan, Q. Xiang, J. Mater. Sci. Technol. 56 (2020) 69–88.
[20] H. Qin, W. Lv, J. Bai, et al., J. Mater. Sci. Technol. 54 (2018) 4811–4820.
[21] M. Wang, Y. Zeng, G. Dong, C. Wang, Chin. J. Catal. 41 (2020) 1498–1510.
[22] Y. Xing, X. Wang, S. Hao, et al., Chin. Chem. Lett. 32 (2021) 13–20.
[23] L. Luo, Z.Y. Gong, J.N. Ma, et al., Appl. Catal. B: Environ. 284 (2021) 119742.
[24] K. Zhao, S. Liu, K. Li, et al., Mol. Catal. 433 (2017) 193–201.
[25] F. Goettmann, A. Fischer, M. Antonietti, A. Thomas, Angew. Chem. Int. Ed. 45 (2006) 4467–4471.
[26] Z. Zeng, K. Li, K. Wei, et al., Chin. J. Catal. 38 (2017) 498–507.
[27] L. Shi, K. Chang, H. Zhang, et al., Small 12 (2016) 4431–4439.
[28] J.D. Hong, X.Y. Xia, Y.S. Wang, R. Xu, J. Mater. Chem. 22 (2012) 15006–15012.
[29] Y. Cui, M. Li, H. Wang, et al., Sep. Purif. Technol. 199 (2018) 251–259.
[30] C. Sun, H. Zhang, H. Liu, et al., Appl. Catal. B: Environ. 235 (2018) 66–74.
[31] J. Zhang, M. Zhang, R.Q. Sun, X. Wang, Angew. Chem. Int. Ed. 51 (2012) 10145–10149.
[32] J. Chen, Z. Hong, Y. Chen, B. Lin, B. Gao, Mater. Lett. 145 (2015) 129–132.
[33] H. Wang, Y. Bian, J. Hu, L. Dai, Appl. Catal. B: Environ. 238 (2018) 592–598.
[34] K. Guan, J. Li, W. Lei, et al., J. Materiomics 7 (2021) 1131–1142.
[35] J. Huang, D. Li, R. Li, et al., Chem. Eng. J. 374 (2019) 242–253.
[36] K. Wang, Q. Li, B. Liu, et al., Appl. Catal. B: Environ. 176-177 (2015) 44–52.
[37] L. Jiang, X. Yuan, G. Zeng, et al., Environ. Sci. Nano 5 (2018) 2604–2617.
[38] A. Hayat, T. Li, Int. J. Energy Res. 43 (2019) 5479–5492.
[39] L. Gao, X. Li, J. Zhao, et al., J. Phys. Chem. Solids 108 (2017) 30–38.
[40] V.R. Battula, S. Kumar, D.K. Chauhan, S. Samanta, K. Kailasam, Appl. Catal. B: Environ. 244 (2019) 313–319.
[41] C. Feng, L. Tang, Y. Deng, et al., Appl. Catal. B: Environ. 281 (2021) 119539.
[42] J. Xu, M. Li, L. Yang, et al., Chem. Eng. J. 394 (2020) 125050.
[43] K.X. Li, Y. Zhong, S.L. Luo, W.Y. Deng, Appl. Catal. B: Environ. 278 (2020) 119313.
[44] Z. Zhou, K. Li, W. Deng, et al., J. Hazard. Mater. 387 (2020) 122023.
[45] Z. Sun, X. Yang, X.F. Yu, et al., Appl. Catal. B: Environ. 285 (2021) 119790.
[46] T. Hou, N. Luo, H. Li, et al., ACS Catal. 7 (2017) 3850–3859.
[47] L.J. Mitchell, C.J. Moody, J. Org. Chem. 79 (2014) 11091–11100.
[48] J. Xu, M. Li, J. Qiu, X.F. Zhang, J. Yao, Int. J. Biol. Macromol. 185 (2021) 297–305.
[49] M. Tian, J. Wen, D. MacDonald, R.M. Asmussen, A. Chen, Electrochem. Commun. 12 (2010) 527–530.
[50] X. Liu, X. Duan, W. Wei, S. Wang, B.J. Ni, Green Chem. 21 (2019) 4266–4289.